Electric Propulsion Characterization for a Stand-Alone Mars CubeSat

IEPC-2019-411

Presented at the 36th International Electric Propulsion Conference
University of Vienna, Austria
September 15-20, 2019

Karthik V. Mani* and Stefano Boccelli†
Politecnico di Milano, Milan, Italy

Francesco Topputo‡
Politecnico di Milano, Milan, Italy

and

Angelo Cervone§
Delft University of Technology, Delft, the Netherlands

Stand-alone CubeSat missions to Mars that escape Earth and experience a deep-space cruise require robust primary propulsion systems for orbit manoeuvring and precise trajectory control. Combined chemical–electric propulsion systems enable a hybrid high-thrust–low-thrust transfer from a high energy Earth orbit to Mars. High-thrust chemical propulsion is used for Earth escape and the low-thrust electric propulsion is used in deep-space cruise, ballsitic capture, and final circularization to an operational orbit about Mars. This work focuses on the performance and design characterization of an iodine-propelled electric propulsion system, concomitant with low-thrust trajectory optimization of the heliocentric transfer and ballistic capture at Mars for a 16U stand-alone CubeSat. A performance model of an inductively coupled miniature ion thruster is implemented to calculate thrust, specific impulse, and efficiencies. A power-constrained low-thrust optimal control problem utilizing the thruster performance is solved to calculate the trajectory, flight time, ΔV, and the propellant consumption for time-optimal and fuel-optimal strategies.

Nomenclature

A	=	Ion thruster cross sectional area [m^2]
A_c	=	Combustion chamber area [m^2]
A_{eff}	=	Effective area for ion and electron wall losses [m^2]
A_{eff1}	=	Effective area for ion wall neutralization [m^2]
A_g	=	Grid area for neutral gas [m^2]
A_{surf}	=	Total surface area [m^2]
A_{sr}	=	Surface recombination area [m^2]
E_g	=	Neutral gas energy [J/m^3]

*PhD Candidate, Department of Aerospace Science and Technology. karthikvenkatesh.mani@polimi.it
†PhD Candidate, Department of Aerospace Science and Technology. stefano.boccelli@polimi.it
‡Associate Professor, Department of Aerospace Science and Technology. francesco.topputo@polimi.it
§Associate Professor, Department of Space Engineering. a.cervone@tudelft.nl

E_e	=	Electron energy [J/m^3]
E	=	Plasma process potential [J]
e	=	Electron charge [C]
g_0	=	Gravitational acceleration [m/s^2]
h_L, h_R	=	Edge-to-centre plasma density ratios
I_{beam}	=	Beam current [A]
I_{sp}	=	Specific impulse [s]
K	=	Collision rate coefficient [m^3/s]
k	=	Wave number
$\mathfrak{M}$	=	Molecular mass [amu]
m	=	Mass [kg]
$\dot{m}$	=	Mass flow rate [kg/s]
n	=	Number density [1/m^3]
p	=	Plasma process power density [W/m^3]
P	=	Power [W]
Q_0	=	Particle flow rate [Pa]
q_{th}	=	Rate of thermal diffusion [W/m^3]
R	=	Radius [m]
r	=	Spacecraft distance [km]
$\mathcal{R}$	=	Resistance [Ω]
T	=	Thrust [N]
$\mathcal{T}_e$	=	Electron temperature [K]
$\mathcal{T}_i$	=	Ion temperature [K]
$\mathcal{T}_g$	=	Neutral gas temperature [K]
$u_{Bohm,i}$	=	Ion bohm velocity [m/s]
V	=	Plasma chamber volume [m^3]
v_g	=	Gas velocity [m/s]
$v_{beam,i}$	=	Ion beam velocity [m/s]
w	=	Particle number density rate due to plasma processes [1/m^{3}s]
β	=	Grid transparency
Γ	=	Particle flux [1/m^{2}s]
ϵ	=	Permittivity [F/m]
η_p	=	Thruster power efficiency
η_m	=	Mass utilization efficiency
η_{tot}	=	Total efficiency
κ	=	Thermal conductivity [W/mK]
κ_B	=	Boltmann constant [J/K]
Λ_0	=	Heat diffusion length [m]
ω	=	Frequency [rad/s]
Ω_{el}	=	Rate of electron-neutral elastic collisions [W/m^3]
Ω_{in}	=	Rate of ion-neutral elastic collisions [W/m^3]

I. Introduction

CubeSats, developed by universities and small-spacecraft consortia, have been used for multifarious Earth-based missions, including Earth observation, climate assessment, biological research.[1] They are placed in very low orbits and have short mission lifetimes. Contemporary CubeSats lack primary propulsion systems and are incapable of performing major orbital maneuvers or precise trajectory control operations. There has been a significant increase in efforts to enhance CubeSat capabilities such as to pursue even more significant scientific research at very low costs.

Development of primary propulsion systems that increase the maneuverability of CubeSats greatly aid in enhancing their capabilities to reach new targets and perform new scientific missions. Some recent mission studies explore micropropulsion options for enabling CubeSats to perform major orbital maneuvers.[2,3] Multiple types of propulsion systems are applicable for CubeSats, namely, chemical, electric, cold gas and warm gas propulsion systems.[4] Chemical propulsion applicable to CubeSats include monopropellant, bipropellant thrusters and solid motors. Electric propulsion options include gridded ion thrusters, Hall thrusters, field emission electric propulsion, pulsed plasma thrusters, and helicon thrusters.[5,6]

Interplanetary CubeSats development is a necessary step for increasing the solar system exploration efforts at a high science-to-investment ratio.[7] CubeSat missions to Mars could be achieved through a) in-situ deployment by a mother ship and b) highly flexible stand-alone Cubesats on deep-space cruise. The MarCO mission, designed by JPL and launched alongside InSight lander mission in May 2018, is the only interplanetary CubeSat in existence.[8] The mission is launched in the interplanetary space from the mother ship and performs a Mars flyby to provide communication support during InSight's landing. The CubeSats use Vacco MiPS (Micro CubeSat Propulsion System) for executing two trajectory control maneuvers. Stand-alone CubeSats to near-Earth objects are shown to be feasible, such as the Miniaturised Asteroid Remote Geophysical Observer (M-ARGO) mission study by the European Space Agency.[9] Improvements to communication, power, and propulsion systems could push the envelope to 1.5 AU, thereby making a stand-alone Mars CubeSat feasible.

Currently, Mars is the holy grail of interplanetary CubeSat missions. Robust primary propulsion systems become indispensable for stand-alone CubeSat missions from Earth to Mars. They increase the launch flexibility and autonomy. A stand-alone CubeSat can be launched alongside any primary payload that is bound for a high-energy Earth orbit, for example Supersynchronous Geostationary Transfer Orbit (SSGTO), as the frequency of such launches is high. From there, the propulsion systems shall enable the CubeSat to escape Earth, perform a heliocentric transfer, achieve ballistic capture and then finally circularize onto an operation orbit about Mars.

Combined chemical–electric propulsion is a key concept that enables stand-alone CubeSats to achieve Earth–Mars transfers by balancing flight time and spacecraft mass.[10] The CubeSat shall escape Earth within a short timeframe using high-thrust chemical propulsion and perform a deep-space cruise using low-thrust electric propulsion. In the extremes lie fully-chemical and fully-electric transfers. A design based on fully-chemical transfers are fast but lead to an excessive system mass. Fully-electric transfers save mass but have untenable transfer times.

This work aims to characterize the electric propulsion system and low-thrust trajectory optimization for post-escape heliocentric transfer towards Mars, ballistic capture, and the final circularization onto an operational orbit about Mars. In this work, section II delineates the mission characteristics of the Mars Atmospheric Radiation Imaging Orbiter (MARIO), a 30 kg 16U CubeSat mission to Mars, and the usage of combined chemical–electric propulsion concomitant with hybrid high-thrust–low-thrust trajectory. In section III, the various types of electric propulsion options for the CubeSat are explored. In section IV a performance model of an iodine-propelled inductively coupled miniature radiofrequency ion thruster[11] is implemented to calculate the performance curves of thrust, specific impulse and efficiencies as a function of input power. The input power varies according to the Sun-spacecraft distance and the power generation capabilities of the CubeSat. In section V, an optimal control problem is solved to compute the low-thrust trajectory, overall ΔV, and the required propellant mass. Section VII presents the conclusions and some details regarding further research.

II. Mission overview

The Mars Atmospheric Radiation Imaging Orbiter (MARIO) is a stand-alone CubeSat exploration mission to Mars that shall demonstrate the capabilities of CubeSats to perform a) orbit raising & Earth escape, b) heliocentric transfer c) ballistic capture at Mars and d) acquisition of the final operating orbit. These are the 4 key phases of this mission. The MARIO mission utilizes combined chemical–electric propulsion systems for executing a hybrid high-thrust–low-thrust trajectory.

The spacecraft is injected into a highly-eccentric Supersynchronous Geostationary Transfer Orbit (SSGTO) with a perigee of 295 km and an apogee of 90,000 km. Some contemporary geostationary satellite missions are launched into SSGTO and then utilize electric propulsion for apogee reduction and circularization to GEO; e.g. Falcon 9 v1.1 rocket launched Thaicom 6 in January 2014 into this orbit and Thaicom 8 in May 2017 into a 350 km $\times$ 90 226 km orbit[a]. Since the number of communication satellite launches (>5 per year) are higher than that of direct deep-space launches ($\sim$1 per year), this orbit is selected to (a) improve the launch opportunities and widen the launch window, (b) reduce the ΔV required for Earth escape, and (c) provide more flexibility and autonomy to the CubeSat mission by diminishing its dependence on larger interplanetary spacecraft.

The presence of Van Allen radiation belts poses a significant risk of radiation damage to the spacecraft. Thus, a swift escape is necessary to avoid excessive damage. A high-thrust chemical propulsion system is used to provide a high ΔV within a short duration for orbit raising and Earth escape. A low-thrust electric propulsion system instead will drastically increase the residence time of the spacecraft in the radiation belts. The maneuvers are split and multiple orbit raisings are pursued to effectively distribute the ΔV and achieve Earth escape within a short timeframe while controlling gravity losses. Figure 1a illustrates the orbit raising and escape using chemical propulsion. The chemical and electric propulsion modules are *two separate systems in the same spacecraft*. Chemical propulsion module comprises a monopropellant thruster that utilizes an Ammoniun Dinitramide (ADN)-based FLP-106 propellant. The characteristics of the chemical propulsion module and the corresponding trajectory for Earth escape is expounded in Ref. 10.

Once Earth escape is achieved, the chemical propulsion is shut-off and the heliocentric transfer to Mars is executed using low-thrust high-specific impulse electric propulsion (Figure 1b). A high-specific impulse system aids in saving valuable system mass and the cruise lasts for $\sim$3.5–4.5 years, culminating with ballistic capture.[12] Two strategies for optimal heliocentric transfer are investigated: a) time-optimal continuous thrusting to minimize flight time and b) fuel-optimal bang-bang thrusting control to minimize propellant consumption. Depending on the mission priority, one of the two techniques can be used. As the Sun-spacecraft distance increases, the generated power decreases and consequently the available power to the thruster decreases. This impacts the specific impulse and thrust.

At the end of the cruise, the spacecraft experiences a *ballistic capture* (Figure 1c): the spacecraft is *captured* into a temporary stable orbit about Mars, only by the virtue of the natural attractions of Mars and the Sun.[12] The orbit acquired by the spacecraft after ballistic capture is highly irregular, and thus unusable for continuous observation missions. A high-thrust maneuver using chemical propulsion is performed to reduce the initial eccentricity and stabilize the orbit. The circularization to 60,000 km orbit is completed through low-thrust propulsion (Figure 1d). At this orbit, the planned thermal camera payload will characterise the temperature in the Mars upper atmosphere.

III. Electric propulsion system

The requirements of the electric propulsion system and the heliocentric transfer are listed in Table 1. The rationale for EP-01 is to set a limit on the maximum transfer time such that the significant scientific observations could be performed before the end of life ($\sim$6 years). The science mission is scheduled for $\sim$6 months and the circularization maneuvers to attain the orbit about Mars takes $\sim$1.2 years (see Section B).

The power generation capability is a function of the Sun-spacecraft distance. EP-02 sets a maximum thruster power consumption since other critical subsystems such as communications, on-board computer, attitude control, and electrical power system operate continuously during the transfer. Both thrust and I_{sp} vary with thruster power P_{th}. Figure 2 illustrates the available and consumed power for the MARIO mission. The total power generation at 1 AU is 175 W and at 1.5 AU is 74.3 W. The combined power consumption

[a]Space Launch Report - Falcon 9
`http://www.spacelaunchreport.com/falcon9ft.html` and `https://www.spacex.com/missions`. Last visited: 24-July-2019

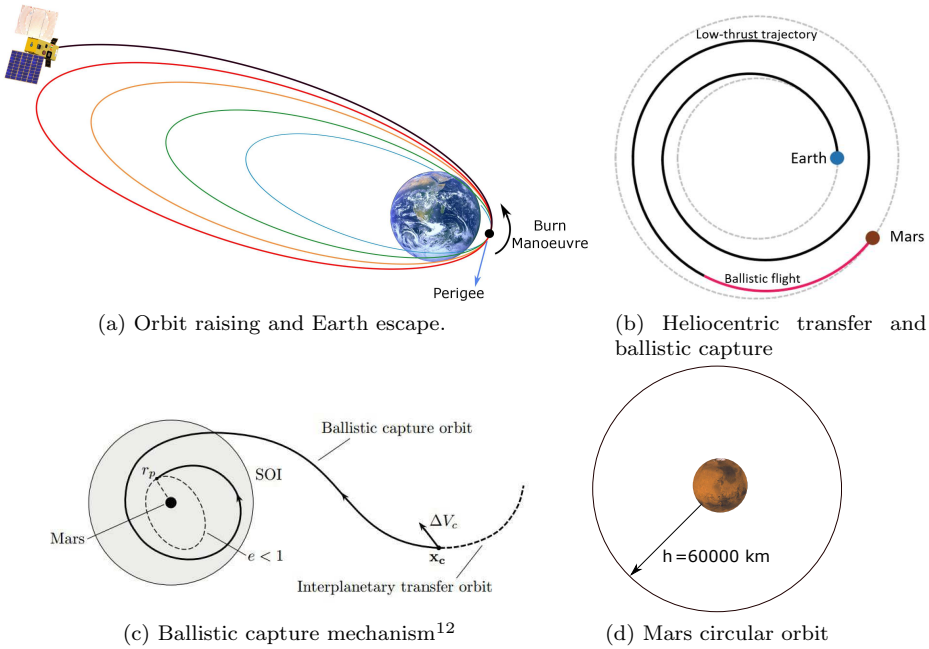

(a) Orbit raising and Earth escape.

(b) Heliocentric transfer and ballistic capture

(c) Ballistic capture mechanism[12]

(d) Mars circular orbit

Figure 1: MARIO Mission Phases

Table 1: Electric propulsion requirements

ID	Requirement
EP-01	The maximum transfer time shall be 4.5 years for cruise and ballistic capture.
EP-02	The system shall have a maximum power consumption of 70 W
EP-03	The total mass of the chemical-electric propulsion systems shall be no more than 15 kg.

of other subsystems is ∼40 W. Cell degradation, neutralization losses and the power processing and control unit (PPCU) consumption (3 W) are included in the thruster input power calculations. The minimum power supplied to the thruster (at ∼1.5 AU) is 30.4 W.

A. System types

Electric propulsion system types in consideration are gridded ion, Hall, field emission electric propulsion, pulsed plasma, and helicon thrusters. The system must be applicable to CubeSats and the thrusts, power consumptions, and the specific impulses vary significantly among system types. A brief comparison is shown in Table 2.

Gridded ion thrusters applicable for small spacecraft have an I_{sp} in the range of 1500-3200 seconds and a propulsion lifetime in the order of 30,000 hours.[13,14] Another suitable option would be the Hall effect thruster which has a lower I_{sp} but higher thrust for the same input power compared to a gridded ion thruster. Field emission electric propulsion (FEEP) thrusters have very high I_{sp} but also have a considerably high power consumption for the thrust produced.[14] Pulsed Plasma Thrusters (PPTs) have low I_{sp} and have a limit on propellant loading. Both, FEEP and PPT have low lifetimes.[14] While considering the heliocentric transfer time and the corresponding thruster operation time (EP-01), both FEEP and PPT are unsuitable for this mission application. Additionally, FEEP uses liquid metals such as cesium, indium and mercury as propellants, whose handling is extremely challenging and hazardous. Helicon thrusters are promising candidates but their low efficiency and lifetime pose a problem. Considering the lifetime, specific impulse and power consumption, the gridded ion thruster is chosen for the analysis and is well suited for MARIO mission application.

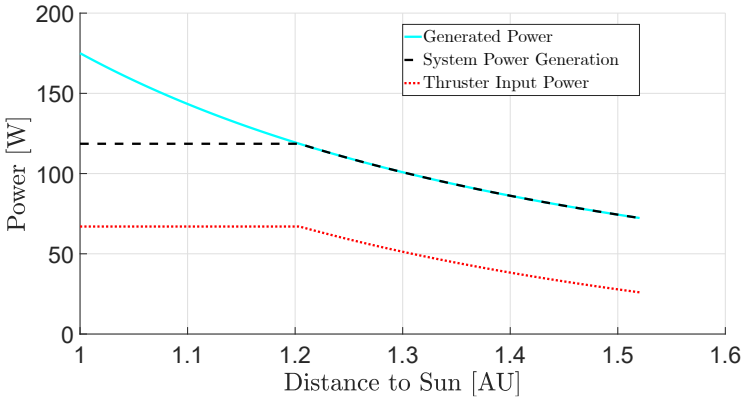

Figure 2: Generated and consumed powers variation with the Sun-spacecraft distance for MARIO mission

Table 2: Comparison of electric propulsion options

Type	**Thrust [mN]**	**I_{sp} [s]**	**Power [W]**	**Life [hours]**
Gridded Ion	0.5-1.6	1500-3200	30-80	∼30000
Hall	1.8-4	800-1400	60-120	∼10000
FEEP	0.35-2	>6000	28-160	<10000
Pulsed Plasma	0.01-1	500-1500	10-30	∼1000
Helicon	0.8-1.5	900-1200	50-80	∼1000

B. Propellant properties

Commonly used propellant in ion thrusters is xenon, a noble gas with a high atomic mass of 131 kg/kmol and a low ionization potential of 12.13 eV. The density of xenon gas is 5.76 kg/m^3 at standard atmospheric conditions. However, xenon is very scarce and occurs only in trace amounts in the atmosphere. It is extracted as a byproduct in the oxygen separation process and is very expensive (∼$1140 per kg). A move towards an alternative propellant that has a similar molecular mass and ionization potential is necessary to reduce the costs while achieving similar performances to xenon.

Iodine (I_2 or I) is a suitable alternative and has a molecular mass of 126.9 kg/kmol (monoatomic). It is a solid in standard atmospheric conditions with a density of 4940 kg/m^3. This eliminates the need for high pressure tanks, complicated plumbing, and sophisticated thermal control systems, which are otherwise required in the case of xenon. Iodine stored in a solid state in compact lightweight tanks can be moderately heated to sublimate and form I_2 vapour. A stand-alone CubeSat on a deep-space cruise to reach Mars requires a high ΔV and subsequently a large propellant mass. Compactness of iodine makes it highly suitable for such CubeSat missions since the propellant can be easily accommodated within the structure. The ionization potentials (E_{iz}) for I_2 and I are 9.3 eV and 10.45 eV, respectively. Thus, it takes less energy to ionize iodine and consequently contributes to a higher electrical efficiency than that of xenon engines. Additionally, the cost of pure iodine is ∼$400 per kg.

Corrosive nature of iodine poses a significant challenge. However, using corrosion-resistant materials like MACOR or Alumina in plasma-generation chambers makes ion thruster compatible with iodine. Thruster grids made out of Nickel–Chromium alloys like Hastelloy or Inconel have high resistance towards iodine corrosion.[15,16] Solar panels and other external surfaces do not suffer from iodine corrosion due to the high vapour pressure of I_2, therefore its condensation is highly unlikely.[17]

IV. Thruster performance model

Characterization of the electric propulsion system for a stand-alone CubeSat to Mars requires a performance model of the thruster and its corresponding application in a low-thrust trajectory optimization framework. A performance model of an iodine-fueled inductively coupled miniature radiofrequency gridded ion thruster is implemented following Grondein et al[11] and Chabert et al[18] to determine the thrust, specific impulse, beam current and efficiencies.

A heat source is utilized to sublimate the solid iodine and generate the I_2 vapour, which is then injected into the chamber. RA cylindrical coil is wound around the plasma chamber and is excited with a radiofrequency (RF) power source. Electromagnetic fields are used to heat the plasma electrons which in turn ionize the neutral gas.[19] A magnetic field is induced in the chamber by the RF coils and there is no permanently applied field. The generated ions are accelerated by a set of DC biased grids.

The design and operational parameters for the performance model are listed in Table 3. The thruster diameter considered here is similar to that of the BIT-3 thruster.[13] A total mass flow rate of 48 μg/s is chosen and the mass flow to the neutralizer cathode is fixed at 10%. The DC grid voltage V_{grid} is set at 2000 V.

Table 3: RF thruster performance model parameters

Parameter	**Value**	**Parameter**	**Value**
Thruster radius, R	1.25 cm	Grid transparency, β	0.6 (ion) & 0.3 (neutral)
Thruster length, L	2.2 cm	Mass flow rate, $\dot{m}_0$	48 μg/s
Chamber volume, V	10.792 cm^3	Particle flow rate, Q_0	1.14×10^{17} s^{-1}
RF coil radius, R_c	1.3 cm	Molecular mass, $\mathfrak{M}$	253.8 (I_2) & 126.9 (I)
No. of coils, N	5	Grid voltage, V_{grid}	2000 V
Grid separation, s	1 mm	Coil resistance, $\mathcal{R}_{coil}$	0.7 Ω

The neutral gas I_2 is injected with a flow rate of Q_0. The ionization process produces positive ions I^+ and I_2^+, and negative ions I^-. Thrust is produced by the acceleration of I_2^+ and I^+ through the grids and I^- doesn't have any direct thrust contribution. Neutral gas thrust is produced by the fluxes of I_2 and I. A set of particle balance equations are written for all species in the model: e^-, I_2, I, I^-, I^+, I_2^+ to calculate their densities (n) as multiple processes take place in the plasma.

The rate coefficients, K, as functions of the electron temperature $\mathcal{T}_e$ are taken from Grondein et al.[11] The processes that take place inside the plasma chamber are ionization (iz), dissociative ionization ($dissiz$), dissociation ($diss$), dissociative attachment ($dissatt$), charge exchange (cex), ion recombination ($ionrec$), and surface recombination (sr). The chemical production rates due to plasma processes appearing in the species balances are: $w_{iz,I} = K_{iz,I}\, n_e\, n_I$ (I ionization), $w_{iz,I2} = K_{iz,I_2}\, n_e\, n_{I_2}$ (I_2 ionization), $w_{dissiz} = K_{dissiz}\, n_e\, n_{I_2}$ (I_2 dissociative ionization), $w_{diss} = K_{diss}\, n_e\, n_{I_2}$ (I_2 dissociation), $w_{dissatt} = K_{dissatt}\, n_e\, n_{I_2}$ (e^-–I_2 dissociative attachment), $w_{cex} = K_{cex}\, n_{I^-}\, n_{I_2^+}$ (I^-–I_2^+ charge exchange), $w_{ionrec} = K_{ionrec}\, n_{I^-}\, n_{I^+}$ (I^-–I^+ recombination). The atomic I surface recombination rate $w_{sr} = \frac{1}{8} n_I v_I \frac{\gamma_{sr}}{1-\gamma_{sr}} \frac{A_{sr}}{V}$. The surface recombination factor γ_{sr} is assumed be 0.02.[11]

$$\dot{n}_e = w_{iz,I} + w_{iz,I_2} + w_{dissiz} - w_{dissatt} - \frac{(\Gamma_{I^+} + \Gamma_{I_2^+})\, A_{eff}}{h_L\, V} \tag{1}$$

$$\dot{n}_{I_2} = \frac{Q_0}{V} - w_{dissiz} - w_{dissatt} - w_{iz,I_2} - w_{diss} + w_{cex} + w_{sr} + \frac{\Gamma_{I_2^+} A_{eff1}}{h_L\, V} - \frac{1}{4}\, n_{I_2}\, v_{I_2} \frac{A_g}{V} \tag{2}$$

$$\dot{n}_I = w_{dissiz} + w_{dissatt} - w_{iz,I} + 2\, w_{diss} + 2\, w_{ionrec} + w_{cex} - 2\, w_{sr} + \frac{\Gamma_{I^+} A_{eff1}}{h_L\, V} - \frac{1}{4}\, v_I\, n_I\, \frac{A_g}{V} \tag{3}$$

$$\dot{n}_{I^-} = w_{dissatt} - w_{ionrec} - w_{cex} \tag{4}$$

$$\dot{n}_{I^+} = w_{iz,I} + w_{dissiz} - w_{ionrec} - \frac{\Gamma_{I^+} A_{eff}}{h_L\, V} \tag{5}$$

$$\dot{n}_{I_2^+} = w_{iz,I_2} - w_{cex} - \frac{\Gamma_{I^+} A_{eff}}{h_L\, V} \tag{6}$$

$A_{eff} = 2\pi R^2 h_L + 2\pi RLh_R$ is the effective area for positive ion and electron wall losses, where h_L and h_R are edge-to-centre plasma denstiy ratios.[18] $A_{eff1} = \pi R^2 (2 - \beta_i) h_L + 2\pi RLh_R$ is the effective area for positive ion wall neutralization. $A_{sr} = \pi R^2 (2 - \beta_g) + 2\pi RL$ is the area for I surface recombination.

Electrons are produced by ionization of I_2 and I, and are lost by dissociative attachment with I_2 and their flux to the chamber walls. Atomic I is produced by the dissociation, dissociative ionization and dissociative attachment of I_2 as well as ion-recombination between I^+ and I^-. It is lost by its ionization, wall recombination and ejection through the grids. Negative ions I^- are produced by dissociative attachment of I_2 and lost by ion-recombination and charge-exchange. Ionization of I and dissociative ionization of I_2 produce I^+ and they are lost by ion-recombination and ion flux through grids. Similarly, I_2^+ are produced by I_2 ionization and lost by charge exchange with I^-.[11]

Neutral gas heating considers energy rates of elastic collisions of electrons–neutrals (Ω_{el}) and ions–neutrals (Ω_{in}) as well as thermal diffusion (q_{th}). The total gas energy $E_g = \frac{3}{2}(n_I + n_{I_2})\kappa_B \mathcal{T}_g$. The energy balance is given by Eq 7.

$$\dot{E}_g = \overbrace{3\frac{m_e}{\mathfrak{M}_I}\kappa_B(\mathcal{T}_e - \mathcal{T}_g)n_e n_I K_{el,I}}^{\Omega_{el,I}} + \overbrace{3\frac{m_e}{\mathfrak{M}_{I_2}}\kappa_B(\mathcal{T}_e - \mathcal{T}_g)n_e n_{I_2} K_{el,I_2}}^{\Omega_{el,I_2}} + \underbrace{\frac{1}{4}n_e\left(n_I\mathfrak{M}_I u^2_{Bohm,I^+}K_{in,I} + n_{I_2}\mathfrak{M}_{I_2}u^2_{Bohm,I_2^+}K_{in,I_2}\right)}_{\Omega_{in}} - \underbrace{\kappa\frac{\mathcal{T}_g - \mathcal{T}_{g0}}{\Lambda_0}\frac{A_{surf}}{V}}_{q_{th}} \quad (7)$$

Here, A_{surf} is the total surface area, κ is the thermal conductivity, κ_B is Boltmann constant, Λ_0 is the heat diffusion length, and $u_{Bohm,i}$ is the ion Bohm velocity.[11] The ion-neutral collision rate factors $K_{in} = \sigma_i v_i$, where σ_i is the global collision cross section set at 10^{-18} m^2 and v_i is the ion velocity expressed as $8\kappa_B\mathcal{T}_i/\pi\mathfrak{M}$.

Power (P_{RF}) supplied to the RF generator is partly absorbed by the plasma and partly dissipated at the coil. The absorbed power density $p_{abs} = \frac{1}{2}\mathcal{R}_{ind}I^2_{coil}/V$, where $\mathcal{R}_{ind}$ is the resistance of an equivalent circuit composed of plasma and the coil.[18] The coil power density $p_{coil} = \frac{1}{2}\mathcal{R}_{coil}I^2_{coil}/V$. The resistances are obtained using a transformer model based on Chabert et al.[18] The $\mathcal{R}_{ind}$ is expressed using Eq. 8

$$\mathcal{R}_{ind} = \frac{2\pi N^2}{L\omega\epsilon_0}\Re e\left[\frac{ikRJ_1(kR)}{\epsilon_p J_0(kR)}\right] \quad (8)$$

Here, k is the wave number and ϵ_p is the plasma complex permittivity. Wave number $k = k_0\sqrt{\epsilon_p}$ and $k_0 = \omega/c$, where ω is the oscillation frequency in radians per second, calculated using the signal frequency set at 13.6 MHz, and c is the speed of light. The complex permittivity ϵ_p is expressed in Eq. 9

$$\epsilon_p = 1 - \frac{\omega_p^2}{\omega(\omega - i\nu_m)} \quad (9)$$

where $\omega_p = \sqrt{n_e e^2/m_e\epsilon_0}$ is the plasma frequency and $\nu_m = n_I K_{el,I} + n_{I_2}K_{el,I_2}$. Quantities e and m_e are electron charge and mass, respectively, while ϵ_0 is the permittivity of free space. The electron power balance is given by Eq. 10. The positive contribution comes from p_{abs}. The electron power is lost due to plasma processes (ionization, dissociation etc.), electron–neutral elastic collisions ($\Omega_{el,I}$ and Ω_{el,I_2}), and ion losses at walls (p_{wall}) and grids (p_{grid}).[11]

$$\dot{E}_e = p_{abs} - p_{iz,I} - p_{iz,I_2} - p_{dissiz} - p_{dissatt} - p_{diss} - p_{exc,I} - \Omega_{el,I} - \Omega_{el,I_2} - p_{wall} - p_{grid} \quad (10)$$

$$\text{with,} \quad p_{wall} = 7\kappa_B\mathcal{T}_e\left(u_{Bohm,I^+}\,n_{I^+} + u_{Bohm,I_2^+}\,n_{I_2^+}\right)\frac{A_{eff} - \pi R^2 h_L}{V}$$

$$p_{grid} = 6\kappa_B\mathcal{T}_e\left(u_{Bohm,I^+}\,n_{I^+} + u_{Bohm,I_2^+}\,n_{I_2^+}\right)\frac{A(1-\beta_i)}{V}$$

The power $p_{iz,I} = E_{iz,I}\,w_{iz,I}$, where $E_{iz,I}$ is the ionization potential of I. Similarly, the rest of the terms are $p_{iz,I_2} = E_{iz,I_2}\,w_{iz,I_2}$, $p_{dissiz} = E_{dissiz}\,w_{dissiz}$, $p_{dissatt} = E_{dissatt}\,w_{dissatt}$, $p_{diss} = E_{diss}\,w_{diss}$

and $p_{exc,I} = E_{exc,I}\, w_{exc,I}$. The terms E_{iz,I_2}, E_{dissiz}, $E_{dissatt}$, E_{diss}, and $E_{exc,I}$ are the potentials of the corresponding plasma processes expressed in Joule.

Particle balance equations Eqs. 1–6, energy balance equation Eq. 7 and the electron power balance equation Eq. 10 are integrated to obtain plasma properties from which the performance values are calculated. The thrust, I_{sp}, and beam current I_{beam} are calculated using fluxes (Γ), ion beam velocities ($v_{beam,i} = \sqrt{2\, e\, V_{grid}/\mathfrak{M}}$), effective grid area of ions ($A\,\beta_i$) and neutrals ($A\,\beta_g$), and the mass flow rate ($\dot{m}_0$).

$$T = \Gamma_i\, \mathfrak{M}\, v_{beam,i}\, A\, \beta_i + \Gamma_g\, \mathfrak{M}\, v_{gas}\, A\, \beta_g \tag{11}$$

$$I_{sp} = \frac{T}{\dot{m}_0\, g_0} \tag{12}$$

$$I_{beam} = e\, \Gamma_i\, A\, \beta_i \tag{13}$$

The ion and neutral fluxes, $\Gamma_i = h_L\, u_{Bohm,i}\, n_i$ and $\Gamma_g = \frac{1}{4}\, v_g\, n_g$, are calculated using positive ion and neutral densities (n), ion Bohm velocities ($u_{Bohm,i} = \sqrt{\mathcal{T}_e\, e/\mathfrak{M}}$), edge-to-centre plasma density ratio (h_L), and neutral gas velocities ($v_g = \sqrt{8\, \kappa_B\, \mathcal{T}_g/\pi\, \mathfrak{M}}$).[18] The fluxes are calculated for ions I_2^+ and I^+, and neutrals gases I_2 and I. The molecular mass $\mathfrak{M}$ is 253.8 amu for I_2 and 126.9 amu for I.

Thruster power efficiency (η_p) is calculated using ion beam power ($P_{beam,i} = I_{beam,i}\, V_{grid}$), neutral gas thrust power ($P_g = \frac{1}{2}\, \mathfrak{M}\, v_g^2\, \Gamma_g\, A\, \beta_g$) and neutralizer cathode power (P_{cath}). The mass utilization efficiency (η_m) is the ratio of ejected ion flow rate ($\Gamma_i\, A\, \beta_i$) and injected gas flow rate (Q_0). Total efficiency is the product of η_p and η_m.

$$\eta_p = \frac{P_{beam,i} + P_g}{P_{beam,i} + P_g + P_{cath} + P_{RF}} \tag{14}$$

$$\eta_m = \frac{\Gamma_i\, A\, \beta_i}{Q_0} \tag{15}$$

$$\eta_{tot} = \eta_p\, \eta_m \tag{16}$$

The input RF power, P_{RF}, supplied to the coils is adjusted according to the available thruster power, P_{th} (see Figure 2). Fluxes Γ_i and Γ_g, and subsequently the powers $P_{beam,i}$ and P_g, depend upon P_{RF}. A simplified neutralizer cathode model based on Richardson's Law of thermionic emission is implemented to calculate the power, P_{cath}, required for ion beam neutralization.[19] The emitter is assumed to be composed of a tungsten filament coated with barium oxide. The emitter temperature $\mathcal{T}_{em}$ is set at 1300 K and the efficiency η_{em} is assumed to be 0.3. The work function of BaO emitter is $W = 1.67 + 2.82 \times 10^{-4} \mathcal{T}_{em}$. The current density emission required for neutralization (Richardson's Law), $J_{rich} = 1.2 \times 10^6\, \mathcal{T}_{em}^2\, \exp\left(-W/(\kappa_B \mathcal{T}_{em})\right)$.[19] The required emitter area $A_{em} = I_{beam}/J_{rich}$ and the corresponding emitter power $P_{em} = A_{em} \sigma_{sb} \mathcal{T}_{em}^4$, where σ_{sb} is the Stefan-Boltzmann constant. The cathode power $P_{cath} = P_{em}/\eta_{em}$.

The total power P_{th} is the sum of $P_{beam,i}$, P_g, P_{cath} and P_{RF}. The variations of thrust, I_{sp} and η with power are illustrated in Figure 3. As the input power increases, the power absorbed by the plasma increases. This results in an increase in ion flux and consequently the thrust. The required neutralization power is 0.63–0.5% of the total power. The mass utilization efficiency increases and the thruster power efficiency decreases with the increase in power. The thruster performance values are listed in Table 4.

Table 4: RF thruster performance at maximum power (67 W)

Parameter	**Value**	**Parameter**	**Value**
Max Thrust, T_{max}	1.49 mN	Mass utilization efficiency, η_m	0.90
Max I_{sp}	3168 s	Power efficiency, η_p	0.49
Max Beam Current, I_{beam}	16.5 mA	Total efficiency, η_{tot}	0.44

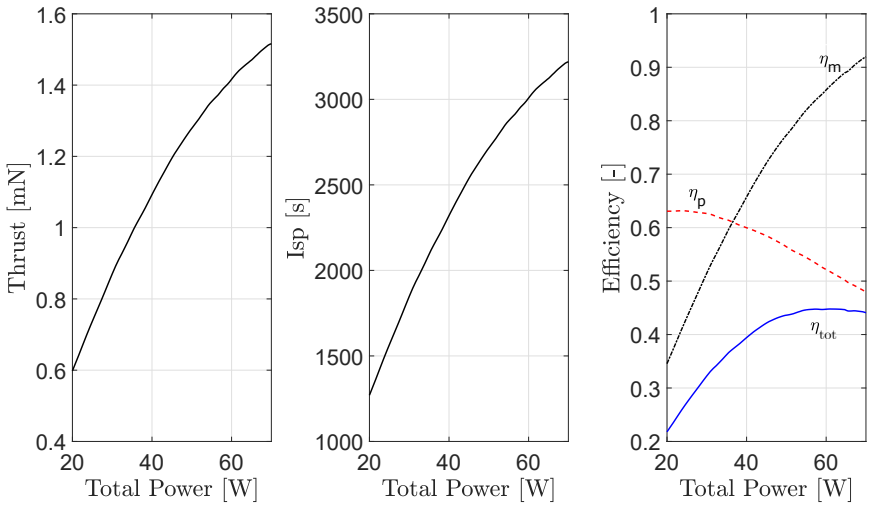

Figure 3: Thrust, $\boldsymbol{I_{sp}}$ and efficiencies vs total power for the considered microthruster

V. Low-thrust trajectory design

A. Heliocentric transfer

Once the final chemical propulsion burn is performed, the spacecraft is set on an escape trajectory. The heliocentric transfer phase begins when the spacecraft is set to depart from a distance of 0.01 AU from Earth (sphere of influence radius), outward on the Sun–Earth line. The target is a defined ballistic capture point at a particular epoch, i.e., when the spacecraft reaches this target point in space at a set epoch, the ballistic capture initiates. Ballistic capture is a phenomenon by which the spacecraft acquires a Mars orbit just by the virtue of natural attractions of Sun and Mars.[12]

The low-thrust trajectory optimization is performed, using the thruster performance, to target this ballistic capture point at a designated epoch. The thruster performance is affected by the thruster input power, which in turn is affected by the Sun-spacecraft distance. The power generation capability is inversely proportional to the square of the distance.

An optimal control problem is solved to minimize a cost function, namely flight time (time-optimal) or propellant consumption (fuel-optimal). Optimization considers real solar system dynamics and solar radiation pressure (SRP).[20] The problem is solved through a direct collocation method to transcribe the optimal control problem to a non-linear programming (NLP) problem. An in-house MATLAB tool called DIRETTO is utilized for transcription of the problem and to supply the NLP solver with the desired inputs.[21] The NLP problem is solved using the Interior Point OPTimizer - IPOPT tool.[22] Mission start and end epochs are defined and the planet ephemerides are obtained through SPICE Toolkit.[23]

The mass of the spacecraft after high-thrust Earth escape is 25.736 kg.[10] The transfer trajectories and the variations of heliocentric eccentricity and semi-major axis for time-optimal and fuel-optimal transfers are illustrated in Figure 4. The time-optimal solution yields a total transfer time of 1200 days ($\sim$ 3.28 years), which satisfies EP-01, and the thruster operation time is 1181.8 days. The fuel-optimal solution yields a transfer time of 1350 days (3.83 years).

The variations of T and I_{sp} for time-optimal and fuel-optimal transfers are illustrated in Figure 5. The quantities α and β pertain to the azimuthal and elevation thrusting angles, defined in the spacecraft body frame. In the fuel-optimal transfer, the thruster is operated intermittently to save propellant mass. It has to be noted that this 'bang-bang' profile is not imposed apriori but rather found as a result of optimization. The overall parameters for the time-optimal and fuel-optimal solutions are shown in Table 5.

For the given total transfer time requirements, the mass savings of the fuel-optimal technique is $\sim$0.41 kg for an additional 150 day flight time. The penalty in flight time is considered quite high for the achieved mass saving. Thus, time-optimal transfer is selected.

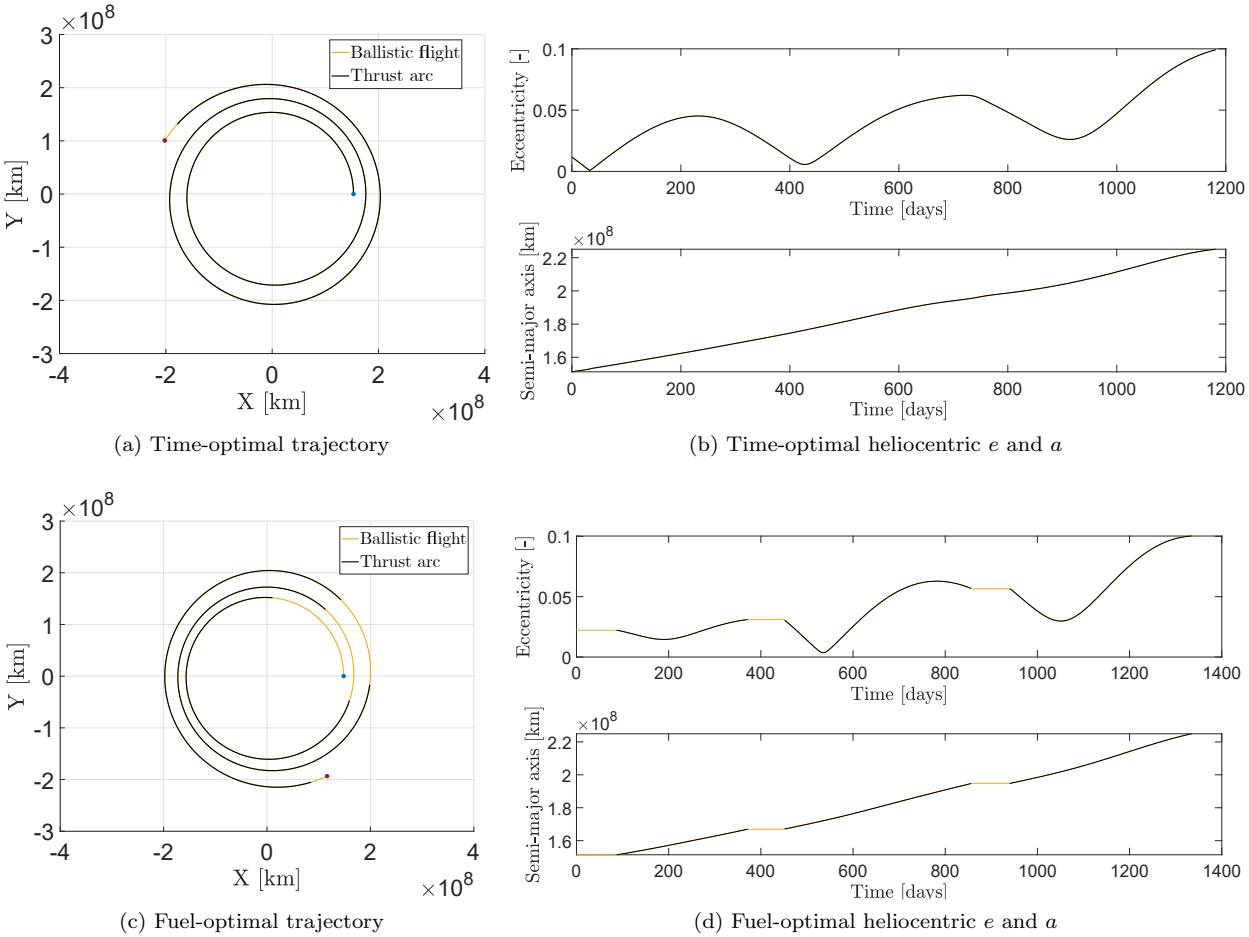

(a) Time-optimal trajectory

(b) Time-optimal heliocentric e and a

(c) Fuel-optimal trajectory

(d) Fuel-optimal heliocentric e and a

Figure 4: Spacecraft heliocentric trajectory, eccentricity $\boldsymbol{e}$ and semi-major axis $\boldsymbol{a}$ variation in time-optimal and fuel-optimal solutions.

B. Ballistic capture and circularization

Once the target point is reached at the designated epoch, the spacecraft ballistically moves towards Mars and acquires a highly highly irregular orbit about Mars, which in nature is not closed and some energy needs to be dissipated to close it. The target points, the epochs, and the corresponding capture orbit orbits are collectively called ballistic capture sets. They are generated using an in-house MATLAB tool, GRATIS.[20] The orbit parameters at the point of capture are $\{a_0, e_0, i_0, \Omega_0, \omega_0, \theta_0\} = \{434600 \text{ km}, 0.99, 22.5°, 0°, 326°, 0°\}$, with the periapsis $r_{p0} = 4346$ km. This orbit is highly inefficient for the scientific observation mission.

The mass of the spacecraft after time-optimal heliocentric transfer is 20.84 kg. Energy dissipation, stabilization, and circularization to a 60000 km orbit are pursued to perform the science mission. The start epoch is set and the chemical propulsion module, with 3 N thurst, provides a retrodirectional ΔV of 45 m/s for stabilization and initial eccentricity reduction. This is done to reduce the overall circularization time since low-thrust propulsion alone would take several years. The orbit parameters after the chemical burn are $\{a, e, i, \Omega, \omega, \theta\} = \{86876 \text{ km}, 0.9499, 22.5°, 360°, 325.8°, 17.88°\}$. This serves as the initial point for low-thrust circularization.

The strategy to circularize around Mars after the chemical burn involves: a) low-thrust eccentricity reduction and initial circularization, b) low-thrust semi-major axis reduction to desired distance, and c) low-thrust final eccentricity reduction/correction. The thruster performance variation with distance is implemented in the analysis. The thrust logic is such that the spacecraft is decelerated when closer to Mars (i.e., $r < a$) to reduce the apoapsis and accelerated when farther away from Mars ($r > a$) to increase the periapsis. This is done until the orbit is circularized at a certain semi-major axis. A constant deceleration is then applied to reduce the semi-major axis to 60000 km altitude and finally, the eccentricity is corrected to reach $e = 0.1$

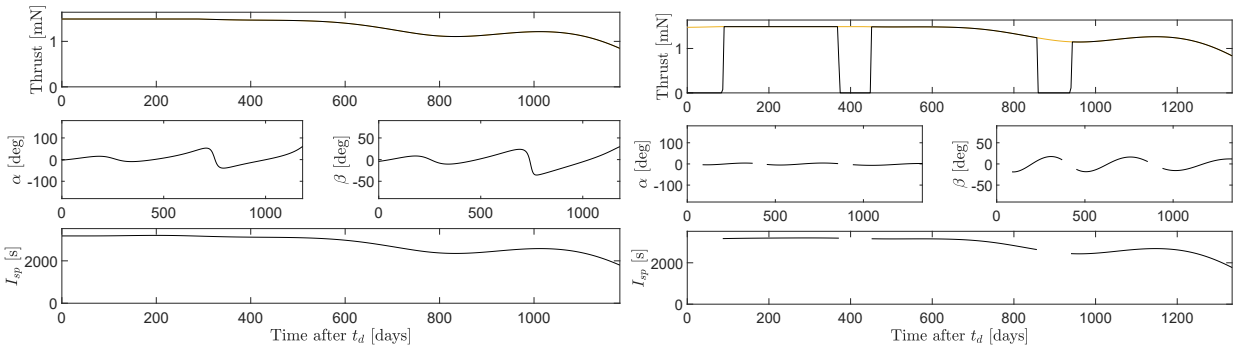

(a) Time-optimal (b) Fuel-optimal

Figure 5: Thrust and I_{sp} variations over time for time-optimal and fuel-optimal solutions

Table 5: Comparison of time-optimal and fuel-optimal heliocentric transfers

Parameter	**Time-optimal**	**Fuel-optimal**
ΔV	5.792 km/s	5.350 km/s
m_p	4.896 kg	4.488 kg
Total Time	1200 days	1350 days
Thrust time	1181.8 days	1334.48 days

and $r = 63390$ km. The cirularization parameters are listed in Table 6. The circularization completes in 432.23 days while consuming 1.793 kg propellant. Time-optimal heliocentric transfer and circularization using electric propulsion last for 1632.23 days cumulatively.

Table 6: Stabilization and circularization parameters

Parameter	**Value**	**Parameter**	**Value**
Chem-prop ΔV_{stab}	45 m/s	Elec-prop ΔV	0.867 km/s
Elec-prop Circ. time	432.23 days	Elec-prop Circ. m_p	1.793 kg

The thrust and the specific impulse for the cirularization maneuvers as well as the trajectory are illustrated in Figure 6.

VI. System sizing

The overall propellant mass required for time-optimal heliocentric transfer and circularization is 6.69 kg. Accommodating for uncertainties, a ∼10% margin is applied on this mass, thus bringing it to 7.4 kg. Iodine solid state density is 4940 kg/m^3 and the corresponding propellant volume is ∼1500 cm^3.

The electric propulsion feed system consists of a propellant reservoir where iodine is stored and sublimated to gas phase (I_2) using a low-power heat source. The resulting vapour is delivered to the thrust chamber using a latch valve and a proportional flow control valve (mass flow control unit).[24] The vapour pressure of iodine is 40 Pa at 25°C. The gas feed line must be heated to prevent iodine from depositing on the surface and keep its vapour state. Owing to the low storage pressure, the reservoir tank is thin walled and made of a thermoplastic material.[13]

The propellant tank is sized to contain solid iodine and the low-power heat source. The heat source is allocated 5% of the tank volume and an additional 5% ullage volume is allocated for the sublimated gas. A total tank volume of 1650 cm^3 is utilized and the corresponding dimensions are 20 cm × 10 cm × 8.25 cm, which is ∼1.7U. The tank mass amounts to 0.02 kg. Considering the feed lines, valves and PPCU, the

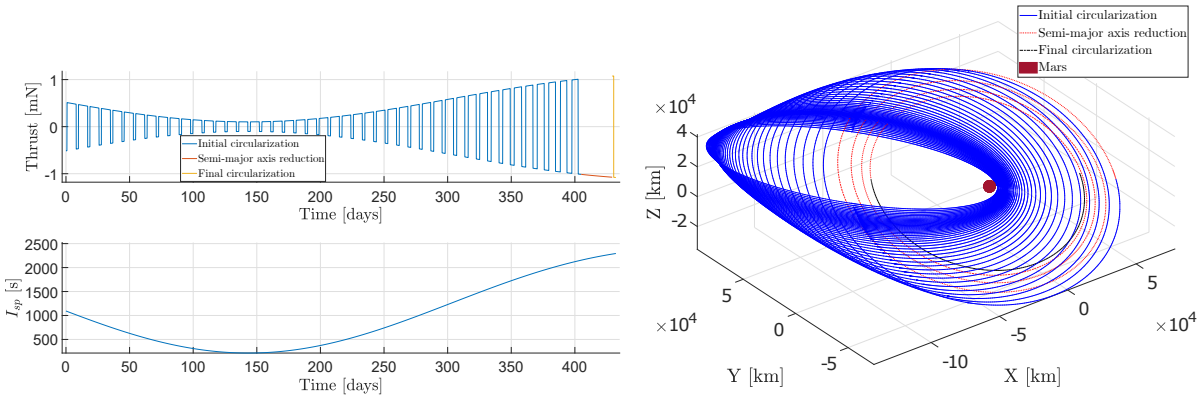

(a) Thrust and I_{sp}

(b) Circularization trajectory

Figure 6: Thrust and $\boldsymbol{I_{sp}}$ variations, and trajectory during circularization to a 60000 km Mars orbit

overall volume of the electric propulsion system is 3U. The schematic of the propulsion system is illustrated in Figure 7. The overall design parameters of the electrical propulsion system are summarized in Table 7.

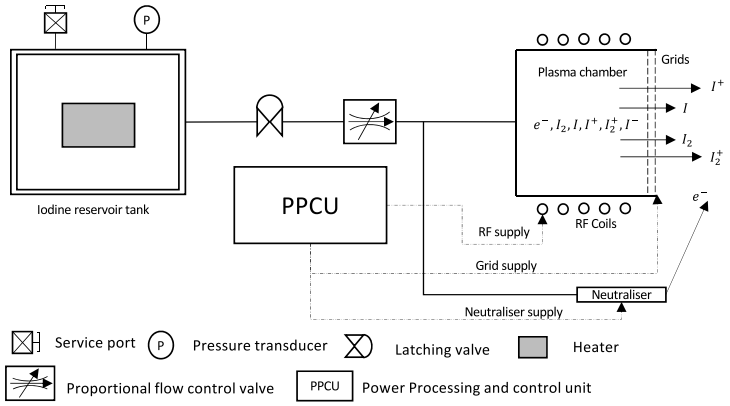

Figure 7: Schematic of the electric propulsion system

Table 7: Electric propulsion design parameters

Parameter	**Value**	**Parameter**	**Value**
Propellant mass, $m_{p,mg}$	7.4 kg	Feed sys. mass, m_{feed}	0.5 kg
PPCU Mass, m_{PPCU}	0.2 kg	Thruster mass, m_T	0.2 kg
Tank volume	1650 cm^3	Tank dimension	20× 10×8.25 cm^3
EP total mass, $m_{ep,sys}$	8.3 kg	EP total volume, $V_{ep,sys}$	3U

VII. Conclusion

Combined chemical–electric propulsion enables stand-alone interplanetary CubeSats to pursue scientifically significant, operations-wise timely, and cost-efficient Solar System exploration missions. The idea is to achieve a balance between flight time and system mass, which is critical for a CubeSat mission. Once the spacecraft is injected into a high-energy Earth orbit, the chemical propulsion module enables orbit raising

and swift Earth escape. The low-thrust electric propulsion enables the heliocentric transfer, ballistic capture, and final circularization to an operational orbit about Mars.

The basis of this work was to characterize the electric propulsion system design, concomitant with low-thrust trajectory optimization for a stand-alone CubeSat to Mars after Earth escape. The electric propulsion stage comprises an iodine-propelled miniature RF ion thruster to execute a deep-space Earth–Mars transfer. A comprehensive global thruster performance model is implemented and the dependence of thrust and I_{sp} on input power are obtained, with maximum values being 1.49 mN and 3168 s, respectively. An optimal control problem is solved for low-thrust trajectory optimization of the Earth–Mars transfer utilizing the calculated RF thruster performances. For the 30 kg 16U CubeSat mission, the electric propulsion systems weighs 8.3 kg (27.66%) and occupies a volume of 3U. The transfer time after Earth escape to a 60000 km Mars circular orbit is 1632.23 days ($\sim$ 4.47 years). The solution is feasible with respect to time and system constraints.

Acknowledgments

This work was pursued in collaboration between Politecnico di Milano and TU Delft. The authors would like to thank Mr. Alvaro Sanz Casado, Mr. Fernando Soler Lanagran, and Mr. Gonçalo Cruz Chambel de Aguiar for their timely and helpful contributions.

References

[1]Thomas H Zurbuchen, Rudolf von Steiger, Sergey Bartalev, Xiaolong Dong, Maurizio Falanga, René Fléron, Anna Gregorio, Timothy S Horbury, David Klumpar, Michael Küppers, et al. Performing high-quality science on cubesats. *Space Research Today*, 196:11–30, Jan 2016.

[2]Ryan W Conversano and Richard E Wirz. Mission capability assessment of cubesats using a miniature ion thruster. *J.Spacecraft Rockets*, 50(5):1035–1046, 2013.

[3]Jennifer Hudson, Sara Spangelo, Andrew Hine, Daniel Kolosa, and Kristina Lemmer. Mission analysis for cubesats with micropropulsion. *Journal of Spacecraft and Rockets*, 53(5):836–846, 2016.

[4]Juergen Mueller, Richard Hofer, and John Ziemer. Survey of propulsion technologies applicable to cubesats. In *Joint Army Navy NASA Air Force (JANNAF) Propulsion Meeting, Colorado Springs, United States*, page 1646, May 2010.

[5]Kristina Lemmer. Propulsion for cubesats. *Acta Astronautica*, 134:231–243, May 2017.

[6]Christopher D Rayburn, Mark E Campbell, and A Thomas Mattick. Pulsed plasma thruster system for microsatellites. *Journal of Spacecraft and Rockets*, 42(1):161–170, 2005.

[7]Robert Staehle, Diana Blaney, Hamid Hemmati, Martin Lo, Pantazis Mouroulis, P Pingree, Thor Wilson, Jordi Puig-Suari, Austin Williams, Bruce Betts, et al. Interplanetary cubesats: opening the solar system to a broad community at lower cost. *Journal of Small Satellites*, 2(1):161–186, 2013.

[8]Andrew Klesh, Brian Clement, Cody Colley, John Essmiller, Daniel Forgette, Joel Krajewski, Anne Marinan, Tomas Martin-Mur, Joel Steinkraus, David Sternberg, et al. MarCO: Early Operations of the First CubeSats to Mars. In *32nd Annual AIAA/USU Conference on Small Satellites, Logan, Utah, United States*, pages 1–10, Aug 2018.

[9]Roger Walker, David Binns, Cristina Bramanti, Massimo Casasco, Paolo Concari, Dario Izzo, Davar Feili, Pablo Fernandez, Jesus Gil Fernandez, Philipp Hager, et al. Deep-space cubesats: thinking inside the box. *Astronomy and Geophysics*, 59(5):5–24, 2018.

[10]Karthik V Mani, Angelo Cervone, and Francesco Topputo. Combined chemical–electric propulsion for a stand-alone mars cubesat. *Journal of Spacecraft and Rockets*, pages 1–15, 2019.

[11]Pascaline Grondein, Trevor Lafleur, Pascal Chabert, and Ane Aanesland. Global model of an iodine gridded plasma thruster. *Physics of Plasmas*, 23(3):033514, 2016.

[12]Francesco Topputo and Edward Belbruno. Earth–Mars transfers with ballistic capture. *Celestial Mechanics and Dynamical Astronomy*, 121(4):329–346, 2015.

[13]Michael Tsay, John Frongillo, and Jurg Zwahlen. Maturation of iodine fueled BIT-3 RF ion thruster and RF neutralizer. In *52nd AIAA - Society of Automotive Engineers - American Society for Engineering Education Joint Propulsion Conference*, page 4544, July 2016.

[14]Stéphane Mazouffre. Electric propulsion for satellites and spacecraft: established technologies and novel approaches. *Plasma Sources Science and Technology*, 25(3):033002, 2016.

[15]Michael Tsay, John J Frongillo III, Joshua Model, and Jurg Zwahlen. Iodine propellant rf ion thruster with rf cathode, 2018. US Patent App. 15/425,317.

[16]Richard D Branam. Iodine plasma (electric propulsion) interaction with spacecraft materials. Technical Report AFRL-AFOSR-VA-TR-2016-0381, The University of Alabama Tuscaloosa & Air Force Research Laboratory, United States, Dec 2016.

[17]Kurt A Polzin, Stephen R Peeples, Joao F Seixal, Stephanie L Mauro, Brandon L Lewis, Gregory A Jerman, Derek H Calvert, John Dankanich, Hani Kamhawi, Tyler A Hickman, et al. Propulsion system development for the iodine satellite (isat) demonstration mission. In *Joint Conference 30th International Symposium on Space Technology and Science, 34th International Electric Propulsion Conference and 6th Nanosatellite Symposium*, pages 1–14, July 2015.

[18]Pascal Chabert, J Arancibia Monreal, Jérôme Bredin, Lara Popelier, and Ane Aanesland. Global model of a gridded-ion thruster powered by a radiofrequency inductive coil. *Physics of Plasmas*, 19(7):073512, 2012.

[19]Dan M Goebel and Ira Katz. *Fundamentals of electric propulsion: ion and Hall thrusters*, volume 1, chapter 4,6, pages 148,251–255. John Wiley & Sons, 2008. ISBN: 978-0470436448.

[20]Gonçalo Aguiar and Francesco Topputo. A technique for designing Earth–Mars low-thrust transfers culminating in ballistic capture. In *7th International Conference on Astrodynamics Tools and Techniques (ICATT)*, pages 1–8, Oberpfaffenhofen, Germany, Nov 2018.

[21]F. Topputo and C. Zhang. Survey of Direct Transcription for Low-Thrust Space Trajectory Optimization with Applications. *Abstract and Applied Analysis*, 1:1–15, June 2014.

[22]Richard H Byrd, Mary E Hribar, and Jorge Nocedal. An interior point algorithm for large-scale nonlinear programming. *Society for Industrial and Applied Mathematics (SIAM) Journal on Optimization.*, 9(4):877–900, 1999.

[23]Charles H Acton Jr. Ancillary data services of nasa's navigation and ancillary information facility. *Planetary and Space Science*, 44(1):65–70, 1996.

[24]Kristof Holste, Waldemar Gärtner, Daniel Zschätzsch, Steffen Scharmann, Peter Köhler, Patrick Dietz, and Peter J Klar. Performance of an iodine-fueled radio-frequency ion-thruster. *European Physical Journal D*, 72(1):9, 2018.